Clustering-based Sensor Placement for Thermal Fault Diagnostics in Large-Format Batteries ⋆

Sara Sattarzadeh. Tanushree Roy. Satadru Dey.

The Pennsylvania State University, University Park, PA 16802 USA
(e-mail: sfs6216@psu.edu, tbr5281@psu.edu, skd5685@psu.edu).

Abstract: Fault detectability and isolability are essential for realizing online diagnostic algorithms in large format batteries used in safety-critical applications. As sensor locations determine such detectability and isolability, sensor placement becomes a crucial task to enable diagnostics. Limited sensing availability in battery systems makes this issue even more challenging. In this setting, we propose an offline sensor placement framework to maximize the fault detectability and isolability based on limited number of given sensors. Within this framework, we combine physics-based thermal model, fault-to-output transfer functions, and data-driven Evidential C-means (ECM) clustering to determine the essential sensor locations. The performance of the proposed framework is demonstrated via simulation studies on a pouch type battery.

Keywords: Batteries, Thermal fault, Sensor placement, Fault detectability, Fault isolability.

1. INTRODUCTION

Thermal faults significantly affect battery safety and performance Xiong et al. (2020); Hu et al. (2020); Tran and Fowler (2020); Bandhauer et al. (2011). Online fault diagnostics algorithms are essential to diagnose these anomalies at an early stage to avoid hazardous situations. Designing these algorithms is anyway challenging in large-format batteries due to the non-uniform temperature distribution. Furthermore, the prerequisite for such algorithms are fault detectability and isolability which in turn depend on battery temperature measurements. In this work, we focus on safety critical applications such as battery-powered devices, vehicles, robots or drones in mining and medical fields Dubaniewicz and DuCarme (2013); Dubaniewicz et al. (2021); Faranda et al. (2019); Ma and Chen (2021); Caldwell et al. (2017); Pu et al. (2015); Bock et al. (2012). In these applications, safety concerns surpass the economical cost of sensors leading to the possibility of multiple temperature sensors. Even with the availability of multiple sensors, the number of sensors is still limited due to installation challenges arising from physical space constraints. Accordingly, these sensors should be placed meaningfully to maximize their utilization. In this context, our goal is to investigate the appropriate sensor locations that would maximize the diagnosis performance.

There is a considerable amount of existing literature on battery thermal fault diagnostics schemes which include the model-based Firoozi et al. (2021); Son and Du (2019); Kang et al. (2020) as well as data-driven approaches Ojo et al. (2020); Hong et al. (2017). The review papers Xiong et al. (2020); Hu et al. (2020); Tran and Fowler (2020) provide a comprehensive list of such existing approaches. There are some works that explores sensor placement for state estimation in arrays or modules of battery cells Samad et al. (2015); Wolf et al. (2012); Sattarzadeh et al. (2021a). However, there are very few works that focus on sensor placement in batteries to increase fault diagnosability. The work in Cheng et al. (2020) utilizes the Dulmage-Mendelsohn (DM) decomposition of the system incidence matrix to detect and isolate the short circuit and sensor faults for single cell and battery packs with minimal sensor set. However, this work does not consider temperature distribution or internal thermal faults within a cell. Authors in Wang et al. (2020) employ the temperature contour and Principle Component Analysis (PCA) to obtain the sensor places in battery packs. However, this work assumes the uniform temperature distribution along each cell. In our recent work Sattarzadeh et al. (2021b), we proposed an optimization based sensor placement approach to maximize the fault detectability and isolability in pouch cell considering two-dimensional temperature distribution. The main contribution of this work Sattarzadeh et al. (2021b) lies in the implementation of partitions of two-dimensional space into as many zones or clusters as there are sensors. Under limited sensor case, instead of providing isolability and detectability of individual fault modes at specific nodes, this formulation provides isolability and detectability of *zonal faults*.

Moreover, the work Sattarzadeh et al. (2021b) has the following limitations. First, it only considers the effect of fault on steady-state output ignoring the transient nature of abrupt or incipient changes. Next, it utilizes an optimization algorithm to simultaneously partition the two-dimensional space into multiple zones and place the sensor at each zone to obtain maximum detectability which

⋆ This work is supported by National Science Foundation under Grants No. 1908560 and 2050315. The opinions, findings, and conclusions or recommendations expressed are those of the author(s) and do not necessarily reflect the views of the National Science Foundation.

has a high computational burden and the computational complexity increases with the size of system.

In this paper, motivated by the approach presented in Blesa et al. (2015), we improve our battery sensor placement approach presented in our previous study Sattarzadeh et al. (2021b). Accordingly, we consider the following enhancements: (i) In order to capture the transient nature of abrupt or incipient faults, we utilize a Fault Sensitivity Matrix (FSM) that contains the residual between faulty and non-faulty model outputs, the zeros and steady state gains of fault-to-output transfer functions. Such FSM captures the transient as well as steady-state effects of faults. It also captures the effect of spatial dynamics of the faults along the cell. (ii) We employed Evidential C-Means (ECM) clustering algorithm to yield a plausibility matrix denoting the probability of nodes belonging to a particular cluster. We utilized these probabilities to partition the two dimensional space into multiple clusters based on FSM. (iii) We propose a simple search algorithm that utilizes the FSM and the clustered nodes to obtain the maximum detectability and isolability. The application of ECM clustering algorithm provides us with statistical knowledge of the impact of faults on each node and enables us to utilize that information in a straight-forward way for both segregation of node clusters as well as sensor placement for maximum detectability and isolability. Unlike our previous work, here the solution of an optimization problem along with a clustering algorithm is rendered unnecessary leading to significantly less computation burden. In other words, the key advantage for our current strategy lies in *detecting zonal faults under a limited sensor scenario using Evidential C-means clustering and Fault Sensitivity Matrix.*

Specifically, the sensor placement methodology is performed in two stages. In the first stage, we utilize the ECM clsutering algorithm to reduce the size of sensor set and generate potential sensor subsets based on the number of available sensors and fault signatures. In the second stage, we utilize the searching algorithm to find the optimum location of sensors in each subsets. As a proof of concept, we consider the single pouch cell battery with high number of discretized nodes in two-dimensional space to illustrate the effectiveness of approach. The paper is organized as follows: Section 2 represents the 2D thermal model of battery, Section 3 discusses the proposed sensor placement strategy, Section 4 represents the simulation results and case studies of the proposed algorithm and the paper is concluded in Section 5.

2. POUCH CELL THERMAL MODEL

In this section, we present the battery model with Partial Differential Equations (PDEs) that captures the two-dimensional thermal behavior of large format pouch cell along length and breadth Yazdanpour et al. (2014):

$$\rho C_p \frac{\partial T}{\partial t} = k_e \left[\frac{\partial^2 T}{\partial x^2} + \frac{\partial^2 T}{\partial y^2} \right] + \frac{\dot{Q}_{total}}{v}, \tag{1}$$

where C_p is the specific heat capacity in $Jkg^{-1}K^{-1}$; k_e is the thermal conductivity of cell in $Wm^{-1}K^{-1}$, and ρ and v are the average density and volume of the cell in kg/m^3 and m^3, respectively. The total heat generated is

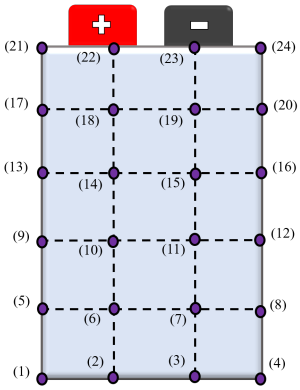

Fig. 1. Discretized nodes of a pouch cell two-dimensional thermal model.

denoted by $\dot{Q}_{total}$ which includes the Ohmic and entropic heat generated inside the cell and the heat convection from the cell to the surrounding area. The term $\dot{Q}_{total}$ can be computed with the knowledge of State-of-Charge, current, open circuit voltage, and terminal voltage of the battery. More explanation on $\dot{Q}_{total}$ computation can be found in Sattarzadeh et al. (2021a). In this model, we assume that the pouch cell is manufactured such that the depth of cell is significantly smaller than the length and breadth of cell. Therefore, we neglect the temperature and heat distribution along the depth of cell and only consider the non-uniform temperature and heat distribution along length and breadth Yazdanpour et al. (2014).

Using method of lines, we discretized the PDE model (1) to a system of (Ordinary Differential Equations) ODEs Sattarzadeh et al. (2021b). A schematic representation of such discretized nodes is shown in Fig. 1. We further rearrange the ODEs to obtain a Linear Time Invariant (LTI) system as follows Sattarzadeh et al. (2021b):

$$\dot{T} = AT + Bu + Ef, \tag{2}$$

$$y = CT, \tag{3}$$

where $u = \dot{Q}_{total}$ is the nominal input, $T = [T_1, T_2, \cdots, T_N]$ is the state vector where the states represent temperature of the discretized nodes, $y = [y_1, y_2, \cdots, y_k]^T$ is the measurement vector, and $f = [f_1, f_2, \cdots, f_m]^T$ represents all possible faults affecting the node temperatures. The matrices A and B are derived from the discretized model, C depends on sensor configuration, and E is the fault distribution matrix. The fault distribution matrix can be formulated from the knowledge of thermal failure modes of the cell. Given the LTI system (2)-(3), our objective is to design a sensor placement strategy to maximize detectability and isolability of internal thermal faults.

3. SENSOR PLACEMENT STRATEGY

In order to apply fault diagnostics algorithms effectively, we need to have insight about the locations of potential faults as well as sensors measurements. However, the diagnosis becomes challenging when the number of faults is more than the number of available measurements Ding (2008). Typically, the number of available sensors are limited due to the cost and installation limitations. Therefore, in this paper we look for a strategy to place k sensors for detection and isolation of m faults where $k < m$. We

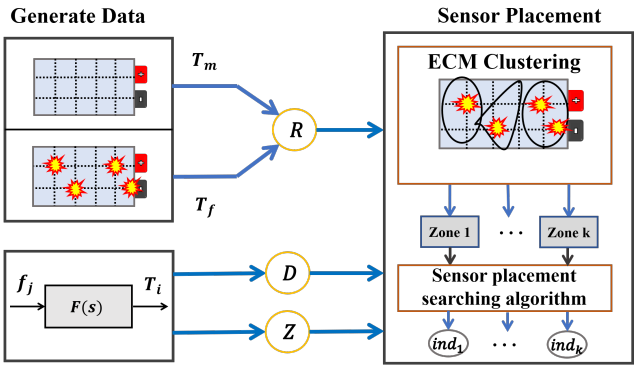

Fig. 2. Sensor placement scheme.

consider the following assumptions: (i) the cost of k sensors installation on battery is the same for any configuration, (ii) the number of sensors, k, is a user defined parameter and is selected based on the trade-off between cost limitation and safety requirements, and (iii) the model represent the physical system with an acceptable accuracy.

We formulate a sensor placement scheme as shown in Fig. 2. The strategy works in two steps. In *Step 1*, we utilize the Evidential C-means (ECM) clustering algorithm to generate k clusters of discretized nodes based on the knowledge of potential faults. Next, in *Step 2*, we apply a searching algorithm to find the optimum location of a sensor within each cluster that maximizes fault detectability and isolability. In the following subsections, we will discuss the generation of Fault Sensitivity Matrix (FSM) used for clustering along with the ECM clustering algorithm in *Step 1*, and the searching algorithm in *Step 2*.

3.1 Fault Sensitivity Matrix

We consider C to be an identity matrix as sensors can potentially be placed in any of the nodes. Subsequently, we formulate the transfer function between j-th fault f_j and i-th output y_i as follows Ding (2008):

$$\mathcal{F}_{i,j}(s) = C_i(sI - A)^{-1}E_j, \tag{4}$$

where E_j is the j-th column of E and C_i is the i-th row of C in (3).

Next, motivated by Blesa et al. (2015), we define the Fault Sensitivity Matrix (FSM), $\mathcal{S}$, as follows:

$$\mathcal{S} = [Z \;\; D \;\; R], \tag{5}$$

The matrix R in (5) is defined as

$$R = \begin{bmatrix} \frac{\partial r_1}{\partial f_1} & \frac{\partial r_1}{\partial f_2} & \dots & \frac{\partial r_1}{\partial f_m} \\ \vdots & \vdots & \dots & \vdots \\ \frac{\partial r_N}{\partial f_1} & \frac{\partial r_N}{\partial f_2} & \dots & \frac{\partial r_N}{\partial f_m} \end{bmatrix}, \tag{6}$$

where $r_i = T_{mi} - T_{f_i}$ is the residual sensitivity capturing the difference between faulty (T_{f_i}) and non-faulty (T_{mi}) temperatures at node i.

The matrix Z in (5) is defined as

$$Z = \begin{bmatrix} z_{1_{f_1}} & z_{1_{f_2}} & \dots & z_{1_{f_m}} \\ \vdots & \vdots & \dots & \vdots \\ z_{N_{f_1}} & z_{N_{f_2}} & \dots & z_{N_{f_m}} \end{bmatrix}, \tag{7}$$

where $Z_{i,j}$ represents the summation of zeros of the transfer function $\mathcal{F}_{i,j}(s)$, that is $(z_{i,j} = \sum_{l=1}^{p} |\mathcal{Z}_l|)$, where p is the number of zeros and $\mathcal{Z}_l$ is the l-th zero of $\mathcal{F}_{i,j}(s)$.

The matrix D in (5) is defined as

$$D = \begin{bmatrix} d_{1_{f_1}} & d_{1_{f_2}} & \dots & d_{1_{f_m}} \\ \vdots & \vdots & \dots & \vdots \\ d_{N_{f_1}} & d_{N_{f_2}} & \dots & d_{N_{f_m}} \end{bmatrix}, \tag{8}$$

where $d_{i,j}$ represents the the absolute value of DC gain of $\mathcal{F}_{i,j}(s)$.

Remark 1. Our goal is to ensure early detection of faults which requires fast transient as well as high steady-state response of the node temperature upon fault occurrence. This requirement dictates the choice of Z, D, and R matrices in (5). The matrix Z considers the zeros of fault-to-output transfer functions which relates to the transient responses. The matrix D captures the steady-state gains on the fault-to-output transfer functions which relates to the strong fault signature at the outputs. Finally, the matrix R captures the difference between faulty and non-faulty temperature responses which would be useful to determine more sensitive nodes.

3.2 Evidential C-means clustering algorithm

We perform the Evidential C-means (ECM) clustering algorithm Masson and Denoeux (2008) to cluster the discretized nodes (potential sensor places) based on the number of available sensors. The ECM algorithm is an unsupervised clustering algorithm which allows the overlapping of clusters as opposed to other clustering algorithms such as K-means clustering. This algorithm provides the probability of membership of each object to all clusters and is helpful in cases where an object is on the boundary of two or more clusters. We utilize this algorithm to cluster the discretized nodes according to their probability of membership in each cluster. The nodes in the same cluster are more similar than the nodes in other clusters. For details of the algorithm, the readers are referred to Masson and Denoeux (2008). In this work, we have used the FSM introduced in the previous subsection to determine the similarity. Specifically, the similarity criterion for clustering is based on the similarity of the rows of FSM. Accordingly, we choose the following features to perform the clustering:

(1) Summation of zeros of the transfer function between output and possible faults. This is captured by Z in (5).
(2) DC gain of fault-to-output transfer function for all possible fault locations. This is captured by D in (5).
(3) Residual between the model output under non-faulty condition and model output under faults. This is captured by R in (5).

We consider all possible sensor locations and extract the aforementioned features to create FSM, $\mathcal{S}$, which serves as the input dataset to ECM. Thereafter, we apply the ECM algorithm on the obtained dataset. The ECM outputs a plausibility matrix of dimension of $N \times k$, given as:

$$P = \begin{bmatrix} p_{1_{\Theta_1}} & p_{1_{\Theta_2}} & \dots & p_{1_{\Theta_k}} \\ \vdots & \vdots & \dots & \vdots \\ p_{N_{\Theta_1}} & p_{N_{\Theta_2}} & \dots & p_{N_{\Theta_k}} \end{bmatrix}, \tag{9}$$

Algorithm 1: Node clustering algorithm.

Input: FSM $\mathcal{S}$ and number of sensors k.
Output: Clusters $(\Theta_1, \ldots, \Theta_k)$ and corresponding nodes.

$P_{N\times k} = ECM(\mathcal{S}, k)$
for $1 \leq i \leq N$ **do**
  $\max_j(p_{i_{\Theta_j}}) \rightarrow$ J
  if $p_{i_{\Theta_J}} = J$ **then**
    $\mathcal{N}_i \in \Theta_l$

where $p_{i_{\Theta_j}}$ represents the probability of node i belonging to cluster Θ_j.

The node clustering algorithm is detailed in Algorithm 1. In Algorithm 1, we have used the following notations: i is the index used for nodes and also for rows of P matrix; $\mathcal{N}_i$ indicates i-th node where $i \in \{1, 2, \cdots, N\}$; Θ_l indicates l-th cluster where $l \in \{1, 2, \cdots, k\}$.

3.3 Search-based sensor placement algorithm

In the previous subsection, the discretized nodes are clustered by ECM. Here, we find the sensor location within each cluster that will maximize fault detectability and isolability based on potential fault locations. With respect to a specific cluster Θ_κ where $\kappa \in \{1, 2, \cdots, k\}$, we denote f_κ to be the set of fault locations in Θ_κ and $\overline{f}_\kappa$ to be the rest of the fault locations that are not in Θ_κ.

In order to obtain the sensor location in each cluster, *first* we consider a vector P_{Θ_κ} which contains the probability of all nodes belonging to cluster Θ_κ. Next, we compute the mean value of elements of P_{Θ_κ}. *Then*, we select those nodes in Θ_κ that have higher probability than the mean value and denote them as the *potential sensor subset* κ for cluster Θ_κ.

Next, we choose particular rows and columns of FSM $\mathcal{S}$ in following two steps. First, we choose only the rows of $\mathcal{S}$ corresponding to the nodes in the *potential sensor subset* κ with all columns and denote it as $\widetilde{S}_{\Theta_\kappa}$. Second, we choose the corresponding columns of $\widetilde{S}_{\Theta_\kappa}$ associated with f_κ and store this selection of rows and columns in a new matrix $\widehat{\mathcal{S}}_{\Theta_\kappa}$. *Subsequently*, we calculate the summation of each rows of $\widehat{\mathcal{S}}_{\Theta_\kappa}$ matrix and denote it as vector $\hat{s}$ with elements $\hat{s}_j$. This quantity $\hat{s}$ captures the signature of f_κ on the *potential sensor subset* κ for cluster Θ_κ.

Then, we choose the corresponding columns of $\widetilde{S}_{\Theta_\kappa}$ associated with $\overline{f}_\kappa$ and store this in a new matrix $\widehat{\mathcal{Q}}_{\Theta_\kappa}$. *Subsequently*, we calculate the summation of each rows of $\widehat{\mathcal{Q}}_{\Theta_\kappa}$ matrix and denote it as vector $\hat{q}$ with elements $\hat{q}_j$. This quantity $\hat{q}$ captures the signature of $\overline{f}_\kappa$ on the *potential sensor subset* κ for cluster Θ_κ.

To ensure detectability and isolability, we select one node from the *potential sensor subset* κ for cluster Θ_κ such that this particular node is sensitive to f_κ and insensitive to $\overline{f}_\kappa$. In other words, the first condition can be achieved by choosing a large element in $\hat{s}$ while the second condition can be achieved by choosing a small element in $\hat{q}$. We achieve this by performing an index search which gives us a common node that satisfies the aforementioned criteria. This sensor placement algorithm is detailed in Algorithm 2.

Algorithm 2: Sensor placement algorithm for maximum detectability and isolability.

Input: $\mathcal{S}_{\Theta_\kappa}$, P_{Θ_κ} and cluster number $\kappa \in \{1, 2, .., k\}$.
Output: Sensor place ind_κ in cluster Θ_κ.

$\text{Mean}(P_{\Theta_\kappa}) \rightarrow M_\kappa$
$\widetilde{\mathcal{S}}_{\Theta_\kappa} = [\,]$.
for $1 \leqslant j \leqslant$ *size*(P_{Θ_κ}) **do**
  if $M_\kappa \leqslant [P_{\Theta_\kappa}]_j$ **then**
    $\left[\widetilde{\mathcal{S}}_{\Theta_\kappa}; [\mathcal{S}_{\Theta_\kappa}]_j\right] \rightarrow \widetilde{\mathcal{S}}_{\Theta_\kappa}$

for $i \in f_\kappa$, $\left[\widetilde{\mathcal{S}}_{\Theta_\kappa}\right]_{j,i} \rightarrow \widehat{\mathcal{S}}_{\Theta_\kappa}$
$\sum_i \left[\widehat{\mathcal{S}}_{\Theta_\kappa}\right]_{j,i} \rightarrow \hat{s}_j$
for $i \in \overline{f}_\kappa$, $\left[\widetilde{\mathcal{S}}_{\Theta_\kappa}\right]_{j,i} \rightarrow \widehat{\mathcal{Q}}_{\Theta_\kappa}$
$\sum_i \left[\widehat{\mathcal{Q}}_{\Theta_\kappa}\right]_{j,i} \rightarrow \hat{q}_j$
$ind_\kappa = \text{argmax}_j(\hat{s}_j - \hat{q}_j)$

4. CASE STUDIES

In this section, we perform case studies to evaluate the performance of proposed sensor placement strategy. We consider the pouch type battery parameters identified in Sattarzadeh et al. (2021a) for this study. Following Sattarzadeh et al. (2021a), the PDE model (1) is discretized into $6\times4 = 24$ nodes as shown in Fig. 1 to obtain the state-space model (2)-(3). We start with generating/formulating the following elements:

(1) We simulated the battery model (2)-(3) in MATLAB platform to generate temperature data at each node under faulty and non-faulty scenarios for all possible fault locations. We have injected white Gaussian type noise in the data to mimic realistic scenario. Subsequently, we subtracted the model data under faulty and non-faulty scenarios to compute the residual $r_i, \forall i \in \{1, 2, \cdots, N\}$. Based on these residuals, we further computed the matrix R in (5).
(2) We used the state-space model (2)-(3) to compute fault-to-output transfer functions $\mathcal{F}_{i,j}(s)$ between j-th fault and i-th output. Furthermore, we computed Z and D in (5) from the transfer functions.

Based on the above elements, we formulate the FSM $\mathcal{S}$ as given in (5). Note that there are two parameters that dictate the outcome of the node clustering algorithm (Algorithm 1): (i) number of sensors k, and (ii) potential fault locations captured by E matrix in (2) which in turn affects the creation of $\mathcal{S}$. In this study, we assume that such potential fault locations are available via thermal failure mode studies. Subsequently, we perform the following case studies to demonstrate the performance of proposed sensor placement algorithm under different scenarios:

(1) **Case 1:** Potential fault locations consist of all nodes (i.e. E is an identity matrix), and two available sensors (i.e. $k = 2$).
(2) **Case 2:** Potential fault locations consist of all nodes (i.e. E is an identity matrix), and three available sensors (i.e. $k = 3$).

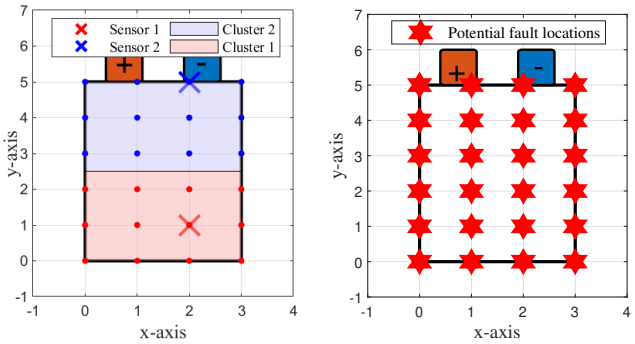

Fig. 3. (a) Clusters and sensor placement result for Case 1 with two available sensors ($k = 2$) and 24 potential faults (at all nodes); (b) potential faults locations.

(3) **Case 3:** Potential fault locations consist of all nodes (i.e. E is an identity matrix), and four available sensors (i.e. $k = 4$).
(4) **Case 4:** Potential fault locations consist of twelve nodes on the bottom half of the cell (i.e. $E = [0_{12}, I_{12}]^T$ where 0_{12} is a null square matrix and I_{12} is an identity matrix) 12 potential node faults close to the bottom of battery cell, and three available sensors (i.e. $k = 3$).

The results of each case studies are shown in Fig. 3 to Fig. 6. In **Case 1** all 24 nodes are considered to be potential hot-spots. The result of proposed sensor placement for two available sensors ($k = 2$) is shown in Fig. 3. The sensors locations for maximum detectability and isolability are shown in Fig. 3a and the potential hot-spots are illustrated in Fig. 3b. The clustered faults in cluster 1 are detectable and isolable through sensor 1 measurement. In other words, in case of fault occurrence at any location of cluster 1, the fault signature will appear in sensor 1 measurement. In **Case 2**, we assume that $k = 3$ and all 24 nodes are considered to be potential hot-spots. The sensors configuration for maximum detectability and isolability are shown in Fig. 4a and the potential fault locations are shown in Fig. 4b. As it can be seen we have three clusters and all the potential faults (nodes) in a specific cluster are detected and isolated by the sensor placed in corresponding cluster. The result of **Case 3** is illustrated in Fig. 5. The condition for potential fault locations in this case study is same as the previous case studies, the only difference is that the number of available measurements is $k = 4$. In **Case 4**, we assume that faults only happen around bottom part of the battery cell. The potential fault locations are shown in Fig. 6b where the hot-spots are considered to be at nodes 1 through 12. Moreover, we assume that we have three available sensors ($k = 3$). The sensor placement result for maximum detectability and isolability is shown in Fig. 6a.

5. CONCLUSION

In this paper, we proposed a clustering-based sensor placement strategy for maximizing fault detectability and isolability in large format pouch cells. The algorithm is performed in two steps. First, we utilized the ECM clustering

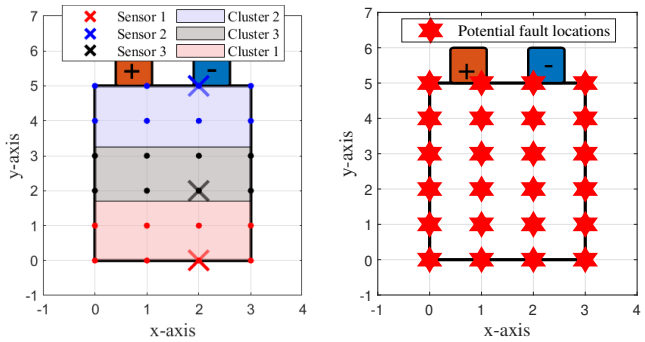

Fig. 4. (a) Clusters and sensor placement result for Case 2 with three available sensors ($k = 3$) and 24 potential faults (at all nodes); (b) potential faults locations.

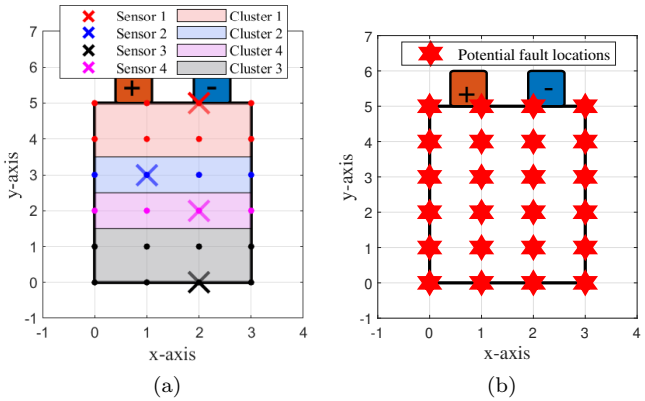

Fig. 5. (a) Clusters and sensor placement result for Case 3 with four available sensors ($k = 4$) and 24 potential faults (at all nodes); (b) potential faults locations.

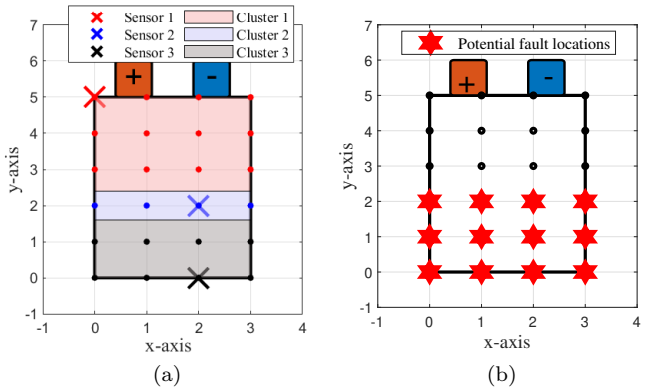

Fig. 6. (a) Clusters and sensor placement result for Case 4 with three available sensors ($k = 3$) and 12 potential faults (around bottom nodes); (b) potential faults locations.

algorithm to cluster the potential sensor places into k clusters based on the number of available measurements and potential hot-spots. Then, we utilized the searching algorithm to find the optimum sensor location in each cluster to satisfy the maximum detectability and isolability. Moreover, this algorithm is helpful in early detection of

fault along the cell by considering the transient response of system to any potential fault. As a proof of concept, we considered the single pouch cell battery with high number of discretized nodes to illustrate the effectiveness of approach. As a future work we plan to examine the robustness of the approach with respect to uncertainties.

REFERENCES

Bandhauer, T.M., Garimella, S., and Fuller, T.F. (2011). A critical review of thermal issues in lithium-ion batteries. *Journal of The Electrochemical Society*, 158(3), R1–R25. doi:10.1149/1.3515880. URL `http://jes.ecsdl.org/content/158/3/R1.abstract`.

Blesa, J., Nejjari, F., and Sarrate, R. (2015). Robust sensor placement for leak location: analysis and design. *Journal of Hydroinformatics*, 18(1), 136–148.

Bock, D.C., Marschilok, A.C., Takeuchi, K.J., and Takeuchi, E.S. (2012). Batteries used to power implantable biomedical devices. *Electrochimica acta*, 84, 155–164.

Caldwell, R. et al. (2017). Hull inspection techniques and strategy-remote inspection developments. In *SPE Offshore Europe Conference & Exhibition*. Society of Petroleum Engineers.

Cheng, Y., D'Arpino, M., and Rizzoni, G. (2020). Structural analysis for fault diagnosis and sensor placement in battery packs. *arXiv preprint arXiv:2008.10533*.

Ding, S.X. (2008). *Model-based fault diagnosis techniques: design schemes, algorithms, and tools*. Springer Science & Business Media.

Dubaniewicz, T.H. and DuCarme, J.P. (2013). Are lithium ion cells intrinsically safe? *IEEE transactions on industry applications*, 49(6), 2451–2460.

Dubaniewicz, T.H., Zlochower, I., Barone, T., Thomas, R., and Yuan, L. (2021). Thermal runaway pressures of iron phosphate lithium-ion cells as a function of free space within sealed enclosures. *Mining, Metallurgy & Exploration*, 38(1), 539–547.

Faranda, R., Bielli, M., Fumagalli, K., et al. (2019). Lithium-ion batteries for explosive atmosphere. In *16th Annual Conference on Petroleum and Chemical Industry Committee (PCIC) Europe*, 1–7.

Firoozi, R., Sattarzadeh, S., and Dey, S. (2021). Cylindrical battery fault detection under extreme fast charging: A physics-based learning approach. *arXiv preprint arXiv:2105.02169*.

Hong, J., Wang, Z., and Liu, P. (2017). Big-data-based thermal runaway prognosis of battery systems for electric vehicles. *Energies*, 10(7), 919.

Hu, X., Zhang, K., Liu, K., Lin, X., Dey, S., and Onori, S. (2020). Advanced Fault Diagnosis for Lithium-Ion Battery Systems: A Review of Fault Mechanisms, Fault Features, and Diagnosis Procedures. *IEEE Industrial Electronics Magazine*, 14(3), 65–91.

Kang, Y., Duan, B., Zhou, Z., Shang, Y., and Zhang, C. (2020). Online multi-fault detection and diagnosis for battery packs in electric vehicles. *Applied Energy*, 259, 114170.

Ma, L. and Chen, Q. (2021). Problems and research on underground charging safety of power battery for coal mine robot. In *IOP Conference Series: Earth and Environmental Science*, volume 651, 032100. IOP Publishing.

Masson, M.H. and Denoeux, T. (2008). Ecm: An evidential version of the fuzzy c-means algorithm. *Pattern Recognition*, 41(4), 1384–1397.

Ojo, O., Lang, H., Kim, Y., Hu, X., Mu, B., and Lin, X. (2020). A neural network-based method for thermal fault detection in lithium-ion batteries. *IEEE Transactions on Industrial Electronics*.

Pu, X., Li, L., Song, H., Du, C., Zhao, Z., Jiang, C., Cao, G., Hu, W., and Wang, Z.L. (2015). A self-charging power unit by integration of a textile triboelectric nanogenerator and a flexible lithium-ion battery for wearable electronics. *Advanced Materials*, 27(15), 2472–2478.

Samad, N.A., Siegel, J.B., Stefanopoulou, A.G., and Knobloch, A. (2015). Observability analysis for surface sensor location in encased battery cells. In *2015 American Control Conference (ACC)*, 299–304. IEEE.

Sattarzadeh, S., Roy, T., and Dey, S. (2021a). Real-time estimation of two-dimensional temperature distribution in lithium-ion pouch cells. *IEEE Transactions on Transportation Electrification*, 1–1. doi:10.1109/TTE.2021.3071950.

Sattarzadeh, S., Roy, T., and Dey, S. (2021b). Thermal fault detection and localization framework for large format batteries. *arXiv preprint arXiv:2103.14229*.

Son, J. and Du, Y. (2019). Model-based stochastic fault detection and diagnosis of lithium-ion batteries. *Processes*, 7(1), 38.

Tran, M.K. and Fowler, M. (2020). A review of lithium-ion battery fault diagnostic algorithms: Current progress and future challenges. *Algorithms*, 13(3), 62.

Wang, J., Hu, D., Shen, H., Yang, T., and Wang, Y. (2020). Optimization methodology for lithium-ion battery temperature sensor placement based on thermal management and thermal runaway requirement. In *2020 11th International Conference on Mechanical and Aerospace Engineering (ICMAE)*, 254–259. IEEE.

Wolf, P., Moura, S., and Krstic, M. (2012). On optimizing sensor placement for spatio-temporal temperature estimation in large battery packs. In *2012 IEEE 51st IEEE Conference on Decision and Control (CDC)*, 973–978. IEEE.

Xiong, R., Sun, W., Yu, Q., and Sun, F. (2020). Research progress, challenges and prospects of fault diagnosis on battery system of electric vehicles. *Applied Energy*, 279, 115855.

Yazdanpour, M., Taheri, P., Mansouri, A., and Bahrami, M. (2014). A distributed analytical electro-thermal model for pouch-type lithium-ion batteries. *Journal of the electrochemical society*, 161(14), A1953.